

Learning Exhaustive Correlation for Spectral Super-Resolution: Where Unified Spatial-Spectral Attention Meets Mutual Linear Dependence

Hongyuan Wang¹ Lizhi Wang¹ Jiang Xu¹
Chang Chen² Xue Hu² Fenglong Song² Youliang Yan²
¹Beijing Institute of Technology ²Huawei Noah's Ark Lab

Abstract

Spectral super-resolution from the easily obtainable RGB image to hyperspectral image (HSI) has drawn increasing interest in the field of computational photography. The crucial aspect of spectral super-resolution lies in exploiting the correlation within HSIs. However, two types of bottlenecks in existing Transformers limit performance improvement and practical applications. First, existing Transformers often separately emphasize either spatial-wise or spectral-wise correlation, disrupting the 3D features of HSI and hindering the exploitation of unified spatial-spectral correlation. Second, the existing self-attention mechanism learns the correlation between pairs of tokens and captures the full-rank correlation matrix, leading to its inability to establish mutual linear dependence among multiple tokens. To address these issues, we propose a novel Exhaustive Correlation Transformer (ECT) for spectral super-resolution. First, we propose a Spectral-wise Discontinuous 3D (SD3D) splitting strategy, which models unified spatial-spectral correlation by simultaneously utilizing spatial-wise continuous splitting and spectral-wise discontinuous splitting. Second, we propose a Dynamic Low-Rank Mapping (DLRM) model, which captures mutual linear dependence among multiple tokens through a dynamically calculated low-rank dependence map. By integrating unified spatial-spectral attention with mutual linear dependence, our ECT can establish exhaustive correlation within HSI. The experimental results on both simulated and real data indicate that our method achieves state-of-the-art performance. Codes and pretrained models will be available later.

1. Introduction

Hyperspectral image (HSI) consists of multiple channels, with each channel representing the response in a specific spectral band. In comparison to the 3-channel RGB image, HSI excels in capturing detailed spectral information from a scene. Owing to this advantage, HSI finds extensive ap-

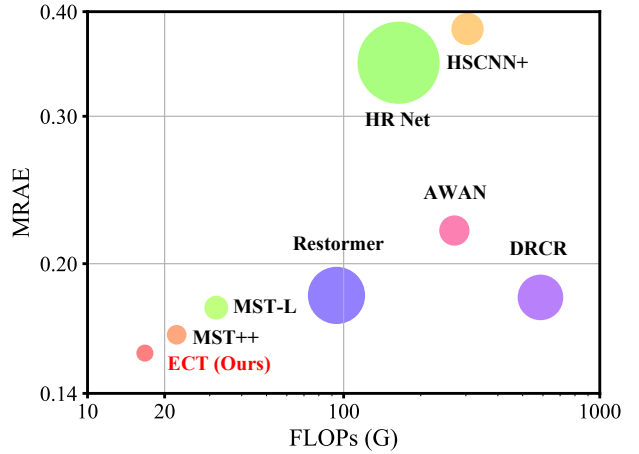


Figure 1. Comparisons of MRAE, FLOPs, and Parameters on the NTIRE 2022 dataset are presented. The circle radius represents the number of parameters. Our Exhaustive Correlation Transformer (ECT) achieves the lowest MRAE with the fewest FLOPs and the smallest number of parameters.

plications in image classification [12, 23, 36], object detection [30], face recognition [57], and more. However, acquiring 3D HSI with 2D sensors is challenging due to the mismatch of dimensions. Traditional scanning-based methods typically require multiple exposures to capture a full HSI, which is disadvantageous for dynamic and rapidly changing scenes.

To address this issue, researchers have designed snapshot compressive imaging (SCI) systems with customized optical modulation and reconstruction algorithms, enabling snapshot acquisition of HSI [8, 26, 43, 47, 52]. However, these methods are often expensive and bulky in system implementation. Consequently, the task of HSI reconstruction from the easily obtainable RGB image [54], known as spectral super-resolution, has emerged as a popular solution.

The crucial aspect of spectral super-resolution lies in exploiting correlations within HSI. Early research utilizes sparse coding [3] or low-rank representation [48] for spec-

tral super-resolution. However, these methods often suffer from limited expressive power and generalization ability, thus failing to achieve satisfactory results. With the increasing computing power, learning-based methods have made significant progress in recent years and have become the mainstream solution for spectral super-resolution. Currently, Transformers [9, 40] have attained the state-of-the-art performance for spectral super-resolution by leveraging spectral-wise correlation through a spectral-wise self-attention mechanism. However, two types of bottlenecks exist that limit performance improvement and practical applications. First, existing Transformers predominantly focus on spectral-wise correlation while overlooking spatial-wise correlation in spectral super-resolution. Some works in other tasks [15, 27, 32, 41] attempt to model both spectral-wise and spatial-wise correlations together but often utilize separate network modules. The neglect and separation undermine the 3D nature of HSI and hinder the exploitation of unified spectral-spatial correlation. Second, the existing spectral-wise self-attention mechanism always learns the correlation between pairs of spectral bands, *i.e.* tokens, and captures the full-rank correlation matrix in the Transformer. These characteristics result in the inability to establish mutual linear dependence among multiple tokens.

In this paper, we propose a novel Exhaustive Correlation Transformer (ECT) to model the unified spatial-spectral correlation and mutual linear dependence, both of which we believe are crucial for spectral super-resolution. The first motivation behind our method stems from the spatial-spectral similarity in HSI. Thus, we propose a Spectral-wise Discontinuous 3D (SD3D) splitting strategy to simultaneously model unified attention along the spectral and spatial dimensions. The SD3D splitting strategy contains continuous splitting in the spatial dimension and discontinuous splitting in the spectral dimension, allowing for an effective focus on spectral-wise non-local features without disrupting the continuous structure in the spatial dimension. The second motivation behind our methods arises from the information redundancy in HSI. Thus, we propose a Dynamic Low-Rank Mapping (DLRM) module to capture the mutual linear dependence among multiple tokens. The DLRM module simultaneously interacts among multiple tokens and maps them into a low-rank space, thereby learning a low-rank dependence map. By integrating unified attention with mutual linear dependence, our ECT can establish the exhaustive correlation within HSI and achieves state-of-the-art in extensive experiments on simulated and real data.

Our contributions are summarized as follows:

- We propose a novel Exhaustive Correlation Transformer (ECT) to model unified spatial-spectral correlation and mutual linear dependence for spectral super-resolution.
- We propose a Spectral-wise Discontinuous 3D (SD3D)

splitting strategy to exploit the unified spatial-spectral correlation within HSI by concurrently adopting spatial-wise continuous and spectral-wise discontinuous splitting.

- We propose a Dynamic Low-Rank Mapping (DLRM) module to model the mutual linear dependence within HSI by dynamically calculating a low-rank dependence map among multiple tokens.
- The experimental results indicate that our method achieves state-of-the-art performance on both simulated and real data, with the lowest error achieved under the lowest computational costs and the smallest number of parameters.

2. Related Work

2.1. Spectral Reconstruction

HSI acquisition is typically carried out using push-broom cameras, which is time-consuming and challenging to capture dynamic or rapidly changing scenes. To address this issue, coded aperture snapshot spectral imaging (CASSI) systems have been widely used, generating 2D measurements [34, 52], which are then processed through a series of reconstruction algorithms [7, 8, 10, 11, 20, 26, 42, 43, 47, 50, 51] to obtain HSI.

However, CASSI systems are often expensive. Reconstructing HSIs from RGB images is a cost-effective alternative. Arad et al. [3] employ sparse coding for spectral super-resolution, while Aeschbacher et al. [1] use shallow learning models and achieve improved results. Due to the presence of substantial redundant information in HSI, a low-rank prior is critical for spectral reconstruction. There are several spectral reconstruction works [16–18, 22, 48, 55, 56] inspired by the low-rank prior. Recently, Three spectral super-resolution challenges [3–5] are held and significantly inspire the research. With the development of deep learning, convolutional neural networks are widely used in the spectral super-resolution task. Shi et al. [37] propose a convolutional neural network for spectral super-resolution, which win the NTIRE 2018 Challenge on Spectral Reconstruction from RGB Images. Li et al. [24, 25] introduce the channel attention mechanism into the convolutional neural network to improve the performance. Thanks to dynamic weights and long-range correlation modeling, Cai et al. [9] are the first to introduce Transformers into the field of spectral super-resolution and win first place in the NTIRE 2022 challenge [5].

2.2. Transformer Model

In the field of NLP, to capture long-range dependencies and enable parallel processing, Vaswani et al. [39] introduced the Transformer model based on the self-attention mechanism. Thanks to its capability to capture long-range depen-

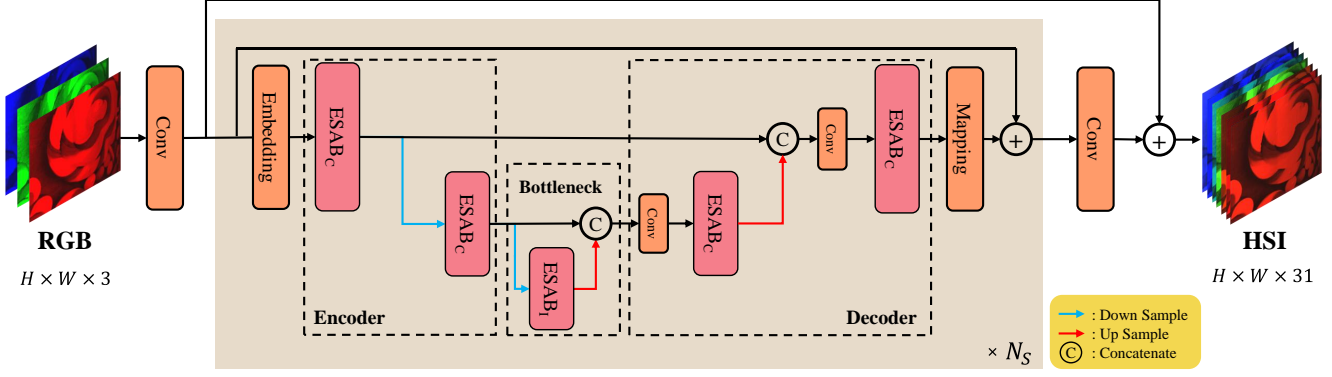


Figure 2. The macro design of Exhaustive Correlation Transformer (ECT).

dencies, global receptive fields, and dynamic weight computation, Dosovitskiy et al. [21] applied the Transformer to image classification, achieving outstanding results. The Transformer architecture has found widespread use in high-level computer vision tasks such as image classification [2, 14, 28, 33, 49], semantic segmentation [35, 38, 46], and object detection [13, 19]. Furthermore, in low-level computer vision tasks, Transformer-based models have also demonstrated remarkable performance in tasks like image super-resolution [15, 29, 31, 60], deraining [44, 45, 53], and denoising [29, 31, 44, 53, 58]. Transformers that leverage the self-attention mechanism can capture long-range correlations between Transformer tokens through dot-product similarity calculations and adaptively fuse tokens based on these correlations, offering strong expressive power.

From the perspective of feature maps, token splitting occurs in the spatial [21, 33] or spectral dimensions [2, 9, 53], allowing for modeling the relationships between pixels or patches or between channels. While there are some efforts to combine these two types of Transformers to model spatial and spectral correlations [15, 27, 32, 41], most of these works directly treat spatial and spectral Transformers as separate modules, which destroys the 3D nature and can not fully exploit the unified correlations.

3. Method

In this section, we first introduce the macro design of the Exhaustive Correlation Transformer (ECT). Then, we delve into the micro design within ECT.

3.1. Macro Design

We propose an Exhaustive Correlation Transformer (ECT) for spectral super-resolution. The overall network employs a multi-stage U-shaped architecture, as shown in Figure 2. For a 3-channel RGB input, it is expanded to 31 channels using a 3×3 convolution and then processed through N_s U-shaped modules. Each U-shaped module consists of Embedding, Encoder, Bottleneck, Decoder, and Mapping com-

ponents. Embedding and Mapping are implemented with 3×3 convolutions, expanding the channel dimensions to 32 on the input side and reducing them back to 31 on the output side. The main components of the Encoder and Decoder are the Cross Exhaustive Self-Attention Blocks ($ESAB_C$), utilizing 4×4 convolutions with a stride of 2 for downsampling and 2×2 transpose convolutions with a stride of 2 for up-sampling. The Bottleneck includes a layer of Inter Exhaustive Self-Attention Block ($ESAB_I$). $ESAB_C$ is employed to model the correlations between tokens, while $ESAB_I$ is used to model the correlations within tokens. $ESAB_C$ can model spatial-wise non-local and global-aware spectral-wise local correlation, while $ESAB_I$ can model spatial-wise local and spectral-wise non-local correlation. The spatial resolution of the feature map becomes $1/4$ after downsampling, while the channel doubles. The number of attention heads scales with the channel changes. Residual connections exist between the Encoder and Decoder, retaining more input information for reconstruction. Furthermore, a long-range residual connection is added to stabilize the training.

3.2. Micro Design

Since the main difference between $ESAB_C$ and $ESAB_I$ lies in the subsequent processing, whether it is for correlations between tokens or within tokens, let us focus on $ESAB_C$ to illustrate the micro design. Furthermore, from this point onward, we will no longer distinguish between $ESAB_C$ and $ESAB_I$ in the mathematical notation below.

As depicted in Figure 3, an Exhaustive Self-Attention Block ($ESAB$) comprises Exhaustive Self-Attention (ESA), Layer Normalization, and a Feed-Forward Network. The key process in ESA is summarized as follows: Firstly, the Spectral-wise Discontinuous 3D ($SD3D$) splitting strategy is applied to generate tokens, facilitating the exploitation of unified spatial-spectral correlation. Following that, the Low-Rank Dependence Map is generated through the Dynamic Low-Rank Mapping ($DLRM$) module to model

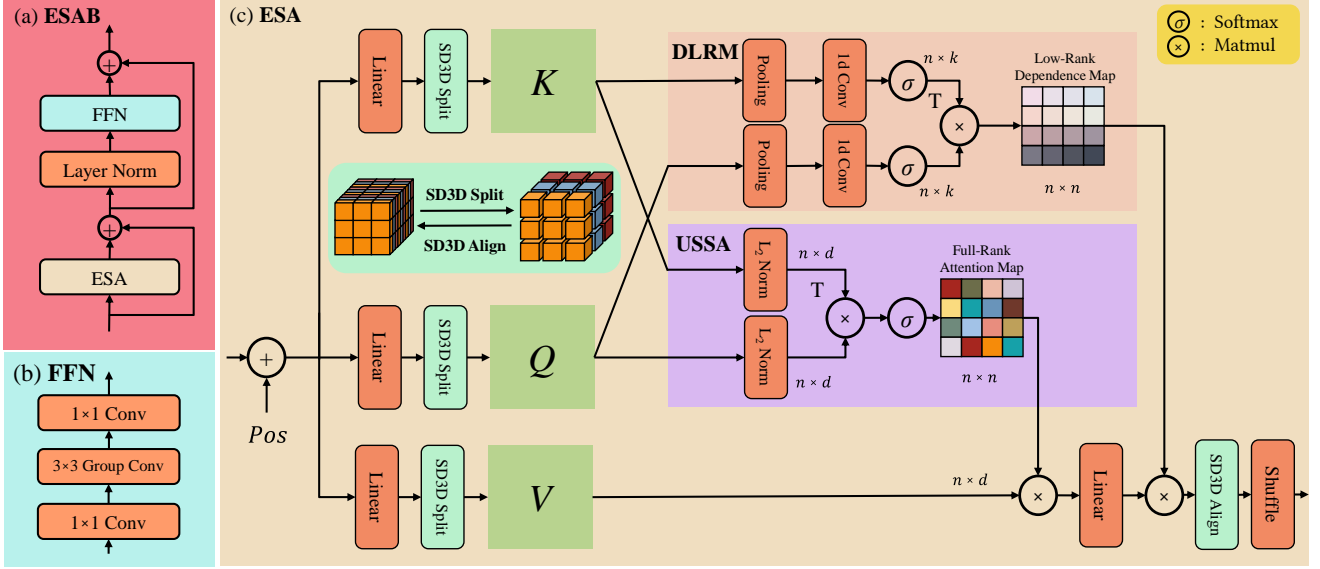


Figure 3. Micro Design of ECT. (a) Exhaustive Self-Attention Block (ESAB). (b) Feed Forward Network (FFN). (c) Exhaustive Self-Attention (ESA). Key designs in ESA are the Spectral-wise Discontinuous 3D (SD3D) splitting and alignment strategies, the Dynamic Low-Rank Mapping (DLRM) model, and the Unified Spatial-Spectral self-Attention (USSA) model.

mutual linear dependence among multiple tokens. The Full-Rank Attention Map is generated through the Unified Spatial-Spectral self-Attention (USSA) module to model the independent correlation between pairs of tokens. Next, we introduce the implementation details of ESA.

First, the feature map undergoes two layers of grouped convolutions to learn dynamic positional encoding, which is added to the feature map to model the position of each token. Then, the feature map is linearly transformed into a hidden space. A Spectral-wise Discontinuous 3D (SD3D) splitting operation is performed to generate Q , K , and V . SD3D splitting strategy contains continuous splitting in the spatial dimension and discontinuous splitting in the spectral dimension, which allows for a more effective focus on spectral-wise non-local features without disrupting the continuous structure in the spatial dimension. The original feature map has dimensions $H \times W \times C$, after the SD3D splitting, the number of tokens, denoted as n , becomes $C \times s/c$, and the dimension of each token, denoted as d , becomes $H \times W \times c/s^2$, where s and c are hyperparameters. To simplify the expression, the multi-head attention mechanism is omitted here.

Then, the Unified Spatial-Spectral self-Attention (USSA) is applied to capture independent full-rank correlations between pairs of tokens. The calculation of the Full-Rank Attention Map in USSA is expressed by

$$\text{USSA}(Q, K) = \sigma \left(\tau \frac{K^T \times Q}{\|K\| \cdot \|Q\|} \right), \quad (1)$$

where σ denotes softmax function and τ is a learnable pa-

rameter. $Q = W_Q X$, $K = W_K X$, and $V = W_V X$. L_2 normalization is performed within each Token to stabilize the training, and then the expressive power is improved by the learnable parameter τ . Since the dimension of tokens d is greater than the number of tokens n in this scenario and the Softmax operation after the dot product, there is a lower risk of rank reduction in the attention maps, as discussed in [6]. Typically, the learned attention maps have a full rank or nearly full rank. From the optimization point of view, since the linear correlation is different in different HSIs, the loss can only be minimized when the attention mechanism learns full-rank or nearly full-rank attention maps. The experiments confirm this point as well, and we will discuss it in the supplementary material. Furthermore, the scaled dot-product attention is calculated independently between paired tokens and cannot capture the mutual linear dependence among multiple tokens.

To address the limitation of self-attention in modeling mutual linear dependence within HSI, we propose a Dynamic Low-Rank Mapping (DLRM) module. The details of DLRM are illustrated in Figure 4. Initially, the tokens from the multi-head Q (K) are restored in a 3D manner and subsequently spatially pooled, reducing the spatial dimensions of the tokens from $h/s \times w/s$ to 2×2 . Following this step, the tokens are flattened in a 3D fashion to form a two-dimensional matrix. Finally, interactions take place among various heads and tokens through a 1d convolution, yielding a feature Q_F (K_F) with dimensions $n \times k$, where k is a hyperparameter and $k < n$. The matrices Q_F and K_F then undergo a Softmax function, followed by transposition and

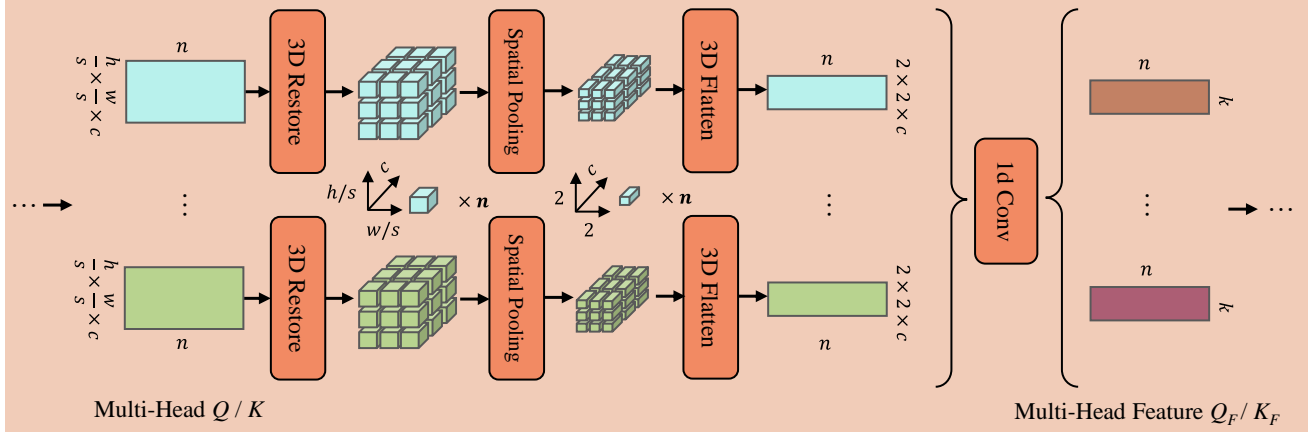


Figure 4. Detailed design of the Dynamic Low-Rank Mapping (DLRM) module.

multiplication to generate a dynamic $n \times n$ matrix, which is a low-rank matrix with a rank no greater than k . The calculation of the low-rank dependence map in DLRM is expressed by

$$\text{DLRM}(Q, K) = \sigma(K_F)^T \times \sigma(Q_F). \quad (2)$$

The difference between the Attention Map in self-attention and the Dependence Map in DLRM is illustrated in Figure 5. As shown in the figure, the calculation of the correlation in self-attention is token-to-token, with each row of the correlation matrix independently calculated. Each element in the matrix is solely associated with two tokens. In contrast, DLRM first facilitates information exchange among various tokens and attention heads. Therefore, each element in the Dependence Map gathers information from multiple tokens. Consequently, each element in the Dependence Map aggregates information from multiple tokens. Moreover, the Dependence Map can implicitly model the linear correlations among multiple tokens due to the low-rank nature. In summary, the Dependence Map can effectively capture the mutual linear dependence among multiple tokens, which is absent in the Attention Map.

Then the correlations learned by USSA and DLRM are used for token fusion. First, V is multiplied by the Full-Rank Attention Map learned by USSA. Following this, V undergoes a linear transformation with the learnable parameter W and is subsequently multiplied by the Low-Rank Dependence Map learned by DLRM. The overall arithmetic process of ESA can be summarized by

$$\text{ESA}(X) = \text{DLRM}(Q, K) \times W \times \text{USSA}(Q, K) \times V. \quad (3)$$

After the token fusion, a Spectral-wise Discontinuous 3D (SD3D) alignment is performed to restore the feature map to its original shape. Finally, channel shuffling is applied to fully explore spectral-wise non-local features.

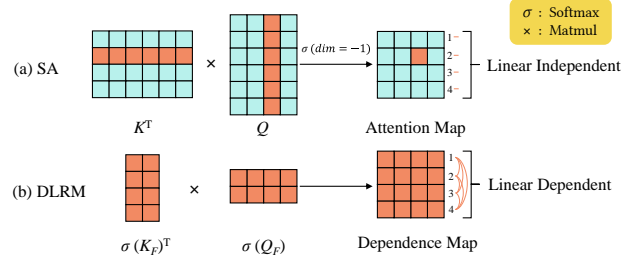


Figure 5. Comparison of the Attention Map in Self-Attention (SA) and the Dependence Map in DLRM.

4. Experiments

4.1. Dataset

For spectral super-resolution experiments on simulated data, we utilized open-source datasets, including NTIRE 2022 [5], NTIRE 2020 Real World Track [4], and ICVL [3]. To further validate the generalization ability of the algorithm, we conduct spectral super-resolution experiments on real RGB data.

For the real data experiments, we capture real RGB images using FLIR Blackfly S BFS-U3-31S4 and obtained the spectral curves of the regions for validation using Specim IQ. We use HSI from the NTIRE 2022 training set and simulate RGB images to create paired training data. RGB simulation and more details about the datasets can be found in the supplementary material.

4.2. Implementation Details

For the hyperparameters in the network structure, we set the SD3D Splitting scale $c = 4$, $s = 2$ and low-rank factor $k = 12$ for ESAB_C. For ESAB_I, we set the SD3D Splitting scale $c = 16$, $s = 4$ and low-rank factor $k = 8$. The number of network stages N_s is set to 2.

Table 1. The experimental results on the NTIRE 2022 dataset, NTIRE 2020 Real World Track dataset, and ICVL dataset are as follows, with **bold** indicating the first place and underlined indicating the second place.

Method	NTIRE 2022 [5]		NTIRE 2020 [4]		ICVL [3]		Params↓	FLOPs↓
	MRAE ↓	RMSE↓	MRAE↓	RMSE↓	MRAE ↓	RMSE↓		
HSCNN+ [37]	0.3814	0.0588	0.0684	0.0182	0.2322	0.0424	4.65 M	304.45 G
HR Net [59]	0.3476	0.0550	0.0682	0.0179	0.1139	0.0313	31.70 M	163.81 G
AWAN [24]	0.2191	0.0349	0.0668	0.0175	0.1040	0.0252	4.04 M	270.61 G
Restormer [53]	0.1833	0.0274	0.0645	0.0157	0.0945	0.0230	15.11 M	93.77 G
DRCR [25]	0.1823	0.0288	0.0664	0.0171	0.0763	0.0164	9.48 M	586.61 G
MST-L [8]	0.1772	0.0256	0.0646	0.0162	0.0728	0.0155	2.45 M	31.82 G
MST++ [9]	<u>0.1645</u>	<u>0.0248</u>	<u>0.0624</u>	<u>0.0155</u>	<u>0.0691</u>	<u>0.0144</u>	<u>1.62 M</u>	<u>22.29 G</u>
ECT (Ours)	0.1564	0.0236	0.0595	0.0146	0.0635	0.0142	1.19 M	16.75 G

For the evaluation metrics, following the NTIRE challenge, we use the Mean Relative Absolute Error (MRAE) and Root Mean Squared Error (RMSE) metrics to evaluate the performance. We primarily use MRAE as the main metric and also adopt it as the training objective. RMSE is used as an auxiliary metric.

For the network training details, we utilize a batch size of 40 and employ a learning rate schedule that follows the cosine annealing scheme, decreasing from $4e-4$ to $1e-6$ over 300k iterations. We choose the AdamW optimizer with parameters $\beta_1 = 0.9$, $\beta_2 = 0.999$, $\epsilon = 10^{-8}$ and weight decay is set to $1e-4$. RGB images are first split into 128×128 patches and undergo random rotations and flips for data augmentation before being input into the network. The codes and pretrained models will be made publicly available.

4.3. Results on Simulated Data

4.3.1 Quantitative Results

On NTIRE 2022 [5], NTIRE 2020 [4], and ICVL [3] datasets, we compared ECT with various neural networks, as presented in Table 1. HSCNN+ is the champion in the NTIRE 2018 Clean Track and Real World Track. HR Net and AWAN are the champions in the NTIRE 2020 Clean track and Real World track, respectively. MST++ and DRCR are the first and third place in NTIRE 2022, respectively. Restormer is an advanced algorithm in image reconstruction. MST-L is a CASSI-based HSI reconstruction algorithm. Among all the methods, ECT achieves the lowest MRAE with the lowest computational costs and the smallest number of parameters, demonstrating the superior performance of our method, and highlighting the significance of modeling unified spatial-spectral correlation and mutual linear dependence.

Table 2. The experimental results on the real data.

Methods	Outdoor Scene		Indoor Scene	
	MRAE↓	RMSE↓	MRAE↓	RMSE↓
DRCR [25]	<u>0.2143</u>	<u>0.0070</u>	0.2499	0.0104
MST++ [9]	0.2622	0.0084	<u>0.2257</u>	<u>0.0091</u>
ECT (Ours)	0.2120	0.0065	0.2095	0.0081

4.3.2 Qualitative Results

We showcase the visual effects of the MRAE heatmaps in Figure 6 and Figure 7. We also present a comparison of spectral curves in small regions among the Ground Truth and various reconstruction algorithms in Figure 8. The visual results indicate that ECT exhibits the best reconstruction performance across different wavelengths, which further confirms the effectiveness of our approach.

4.4. Results on Real Data

To further investigate the generalization ability of ECT, we conduct some experiments on real RGB data. We capture RGB images of a color chart both indoors under halogen lights and outdoors under sunlight, along with corresponding HSIs. We evaluated the algorithms using the average error of the 18 color patches on the color chart. The quantitative and qualitative results of ECT compared with two advanced spectral super-resolution methods MST++ [9] and DRCR [25] are shown in Table 2 and Figure 9. The experimental results on real data demonstrate the advanced performance and the strong generalization ability of our ECT.

4.5. Ablation Study

To fully explore the effects and the working mechanics of the Spectral-wise Discontinuous 3D (SD3D) splitting strat-

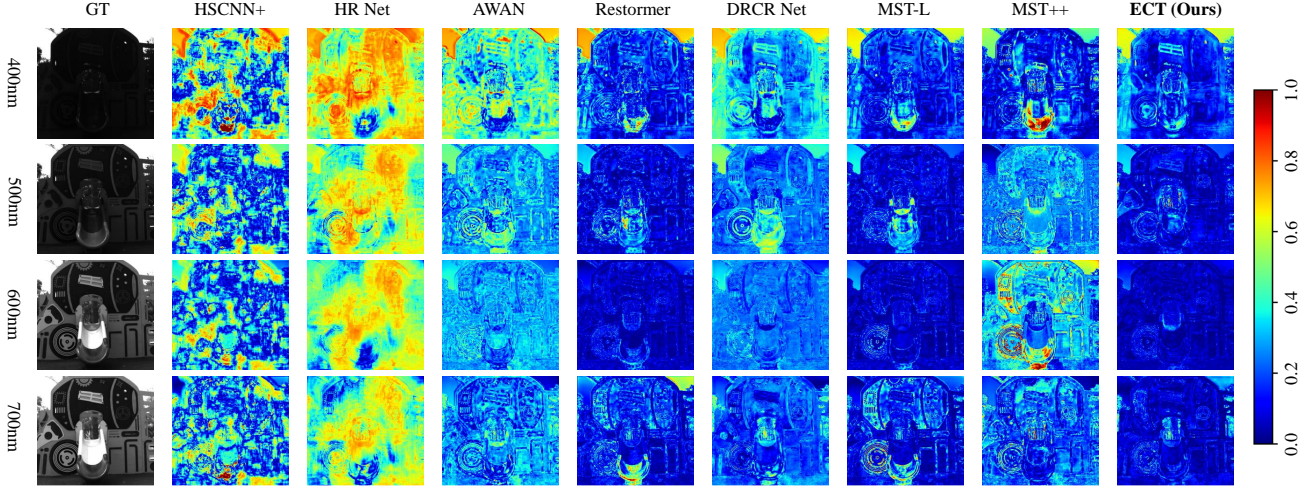


Figure 6. The MRAE heatmaps, including 400nm, 500nm, 600nm, and 700nm bands on *ARAD_0944* from the NTIRE 2022 validation data.

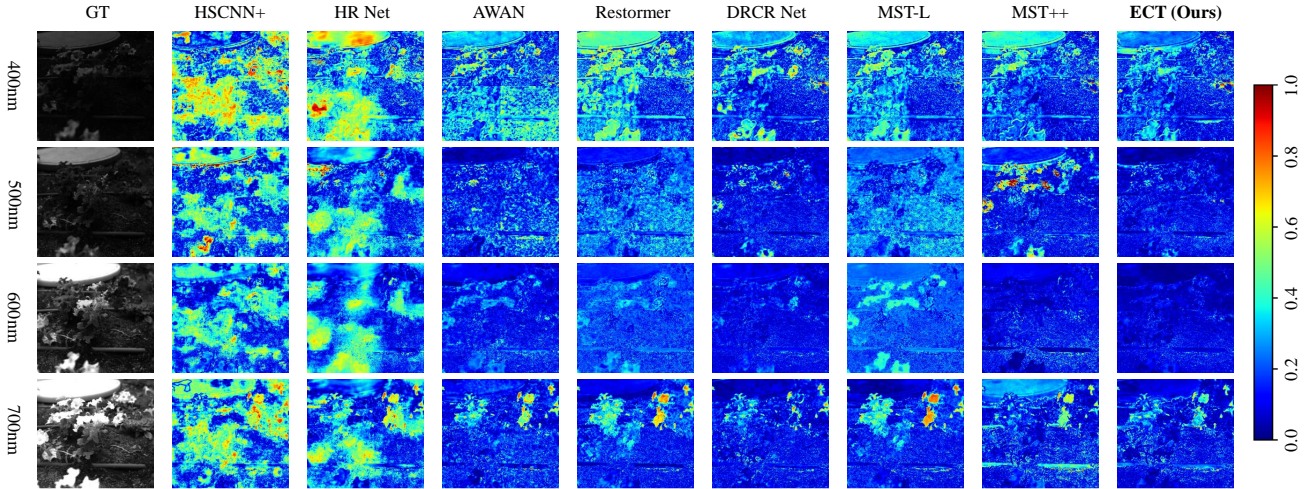


Figure 7. The MRAE heatmaps, including 400nm, 500nm, 600nm, and 700nm bands on *ARAD_0940* from the NTIRE 2022 validation data.

egy and the Dynamic Low-Rank Mapping (DLRM) module, we introduce some ablation studies here. More ablation studies can be found in the supplementary material. All ablation studies are conducted on the NTIRE 2022 dataset with a one-stage U-shaped net.

4.5.1 Ablation Study of SD3D Splitting and DLRM

The Spectral-wise Discontinuous 3D (SD3D) splitting strategy and the Dynamic Low-Rank Mapping (DLRM) are our two significant contributions. The SD3D splitting strategy is used to model unified spatial-spectral correlation, while DLRM is employed to capture mutual linear dependence. The experimental results, as shown in Table 3, demonstrate

Table 3. Ablation study of SD3D splitting strategy and the DLRM module.

SD3D	DLRM	MRAE↓	RMSE↓	Params↓	FLOPs↓
✗	✗	0.1761	0.0266	0.55M	7.84G
✓	✗	<u>0.1700</u>	<u>0.0255</u>	0.58M	8.24G
✗	✓	0.1733	0.0261	0.56M	8.27G
✓	✓	0.1665	0.0246	0.60M	8.69G

that both the SD3D splitting strategy and DLRM can lead to improvements. When used together, they achieve even greater performance improvements.

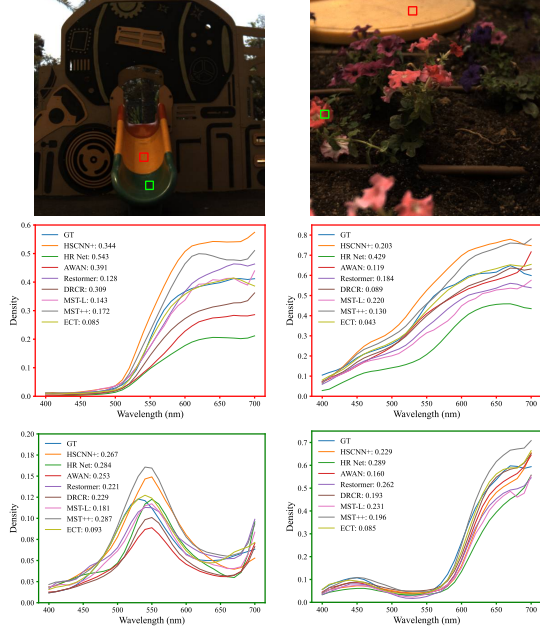


Figure 8. Comparison of reconstructed spectral curves and MRAE in the small regions. The images in the first line are the official RGB of ARAD_0944 and ARAD_0940 from the NTIRE 2022 validation data. The spectral curves with the red and green axes correspond to the red and green boxes in the corresponding figure.

Table 4. Ablation study of the SD3D splitting strategy.

Spatial-wise	Spectral-wise	MRAE↓	RMSE↓
Continuous	Continuous	0.1769	<u>0.0263</u>
Continuous	Discontinuous	0.1665	0.0246
Discontinuous	Discontinuous	<u>0.1739</u>	<u>0.0263</u>

4.5.2 Ablation Study of SD3D Splitting Strategy

The key characteristic of the SD3D splitting strategy lies in its spatial-wise continuity and spectral-wise discontinuity splitting approach. Discontinuous splitting allows for a greater focus on non-local information, while continuous splitting helps preserve the local structure. We conducted an ablation study on the continuity and discontinuity in both spectral and spatial directions, as shown in Table 4. Experiments indicate that spectral super-resolution benefits from non-local features in the spectral direction, and adverse effects arise when disrupting spatial continuity.

4.5.3 Ablation Study of Low-Rank Factor k

The critical parameter in the DLRM module is the number of feature Q_F (K_F) columns, denoted as k . The rank of the low-rank dependence map in DLRM is not greater than k . The experimental results for different values of k in ESAB_C

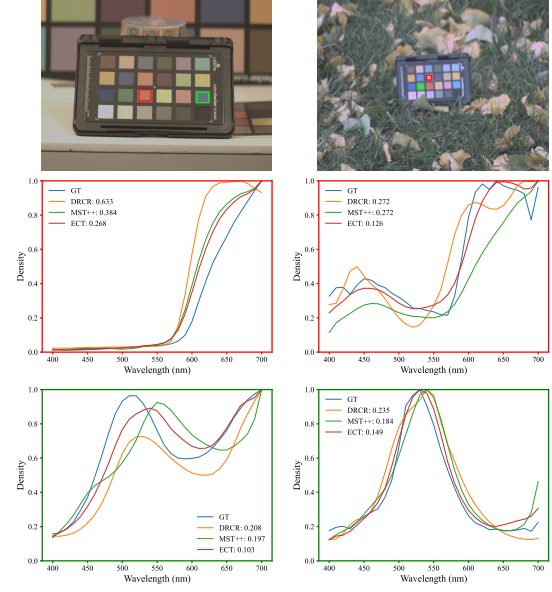


Figure 9. Comparison of reconstructed spectral curves and MRAE in the small regions. Each region is normalized to remove the influence of brightness. The images in the first line are the real RGBs captured indoors and outdoors. Please zoom in.

Table 5. Ablation study of the low-rank factor k .

Fac. k	MRAE↓	RMSE↓	Params↓	FLOPs↓
8	0.1689	0.0260	0.60M	8.69G
12	0.1665	0.0246	0.60M	8.69G
16	<u>0.1671</u>	<u>0.0249</u>	0.60M	8.69G
32	0.1701	0.0259	0.62M	8.69 G

are shown in Table 5. When $k = 32$, it means $k = n$, which does not constrain the dependence map to be low-rank. The experimental results highlight the importance of the low-rank characteristic of the dependence map.

5. Conclusion

In this paper, we analyze the limitations of existing spectral super-resolution Transformers in modeling unified spatial-spectral correlation and mutual linear dependence. We propose a novel Exhaustive Correlation Transformer (ECT) to model these correlations for spectral super-resolution. Specifically, we propose a Spectral-wise Discontinuous 3D (SD3D) splitting strategy to model unified spatial-spectral correlation and a Dynamic Low-Rank Mapping (DLRM) module to capture mutual linear dependence. Experimental results demonstrate that our approach achieves state-of-the-art performance on both simulated and real data. In future work, we will commit to applying our method to other tasks related to hyperspectral imaging.

References

- [1] Jonas Aeschbacher, Jiqing Wu, and Radu Timofte. In defense of shallow learned spectral reconstruction from rgb images. In *ICCVW*, pages 471–479, 2017. [2](#)
- [2] Alaaeldin Ali, Hugo Touvron, Mathilde Caron, Piotr Bojanowski, Matthijs Douze, Armand Joulin, Ivan Laptev, Natalia Neverova, Gabriel Synnaeve, Jakob Verbeek, et al. Xcit: Cross-covariance image transformers. *NeurIPS*, 34:20014–20027, 2021. [3](#)
- [3] Boaz Arad and Ohad Ben-Shahar. Sparse recovery of hyperspectral signal from natural rgb images. In *ECCV*, pages 19–34. Springer, 2016. [1](#), [2](#), [5](#), [6](#)
- [4] Boaz Arad, Radu Timofte, Ohad Ben-Shahar, Yi-Tun Lin, and Graham D Finlayson. Ntire 2020 challenge on spectral reconstruction from an rgb image. In *CVPRW*, pages 446–447, 2020. [5](#), [6](#)
- [5] Boaz Arad, Radu Timofte, Rony Yahel, Nimrod Morag, Amir Bernat, Yuanhao Cai, Jing Lin, Zudi Lin, Haoqian Wang, Yulun Zhang, et al. Ntire 2022 spectral recovery challenge and data set. In *CVPRW*, pages 863–881, 2022. [2](#), [5](#), [6](#)
- [6] Srinadh Bhojanapalli, Chulhee Yun, Ankit Singh Rawat, Sashank Reddi, and Sanjiv Kumar. Low-rank bottleneck in multi-head attention models. In *ICML*, pages 864–873. PMLR, 2020. [4](#)
- [7] Yuanhao Cai, Jing Lin, Xiaowan Hu, Haoqian Wang, Xin Yuan, Yulun Zhang, Radu Timofte, and Luc Van Gool. Coarse-to-fine sparse transformer for hyperspectral image reconstruction. In *ECCV*, pages 686–704. Springer, 2022. [2](#)
- [8] Yuanhao Cai, Jing Lin, Xiaowan Hu, Haoqian Wang, Xin Yuan, Yulun Zhang, Radu Timofte, and Luc Van Gool. Mask-guided spectral-wise transformer for efficient hyperspectral image reconstruction. In *CVPR*, pages 17502–17511, 2022. [1](#), [2](#), [6](#)
- [9] Yuanhao Cai, Jing Lin, Zudi Lin, Haoqian Wang, Yulun Zhang, Hanspeter Pfister, Radu Timofte, and Luc Van Gool. Mst++: Multi-stage spectral-wise transformer for efficient spectral reconstruction. In *CVPRW*, pages 745–755, 2022. [2](#), [3](#), [6](#)
- [10] Yuanhao Cai, Jing Lin, Haoqian Wang, Xin Yuan, Henghui Ding, Yulun Zhang, Radu Timofte, and Luc V Gool. Degradation-aware unfolding half-shuffle transformer for spectral compressive imaging. *NeurIPS*, 35:37749–37761, 2022. [2](#)
- [11] Yuanhao Cai, Yuxin Zheng, Jing Lin, Haoqian Wang, Xin Yuan, and Yulun Zhang. Binarized spectral compressive imaging. *arXiv preprint arXiv:2305.10299*, 2023. [2](#)
- [12] Gustavo Camps-Valls and Lorenzo Bruzzone. Kernel-based methods for hyperspectral image classification. *IEEE TGRS*, 43(6):1351–1362, 2005. [1](#)
- [13] Nicolas Carion, Francisco Massa, Gabriel Synnaeve, Nicolas Usunier, Alexander Kirillov, and Sergey Zagoruyko. End-to-end object detection with transformers. In *ECCV*, pages 213–229. Springer, 2020. [3](#)
- [14] Chun-Fu Richard Chen, Quanfu Fan, and Rameswar Panda. Crossvit: Cross-attention multi-scale vision transformer for image classification. In *ICCV*, pages 357–366, 2021. [3](#)
- [15] Xiangyu Chen, Xintao Wang, Jiantao Zhou, Yu Qiao, and Chao Dong. Activating more pixels in image super-resolution transformer. In *CVPR*, pages 22367–22377, 2023. [2](#), [3](#)
- [16] Renwei Dian and Shutao Li. Hyperspectral image super-resolution via subspace-based low tensor multi-rank regularization. *IEEE TIP*, 28(10):5135–5146, 2019. [2](#)
- [17] Renwei Dian, Leyuan Fang, and Shutao Li. Hyperspectral image super-resolution via non-local sparse tensor factorization. In *CVPR*, pages 5344–5353, 2017.
- [18] Renwei Dian, Shutao Li, and Leyuan Fang. Learning a low tensor-train rank representation for hyperspectral image super-resolution. *IEEE TNNLS*, 30(9):2672–2683, 2019. [2](#)
- [19] Jian Ding, Nan Xue, Yang Long, Gui-Song Xia, and Qikai Lu. Learning roi transformer for oriented object detection in aerial images. In *CVPR*, pages 2849–2858, 2019. [3](#)
- [20] Yubo Dong, Dahua Gao, Tian Qiu, Yuyan Li, Minxi Yang, and Guangming Shi. Residual degradation learning unfolding framework with mixing priors across spectral and spatial for compressive spectral imaging. In *ICCV*, pages 22262–22271, 2023. [2](#)
- [21] Alexey Dosovitskiy, Lucas Beyer, Alexander Kolesnikov, Dirk Weissenborn, Xiaohua Zhai, Thomas Unterthiner, Mostafa Dehghani, Matthias Minderer, Georg Heigold, Sylvain Gelly, et al. An image is worth 16x16 words: Transformers for image recognition at scale. *arXiv preprint arXiv:2010.11929*, 2020. [3](#)
- [22] Ying Fu, Yinqiang Zheng, Imari Sato, and Yoichi Sato. Exploiting spectral-spatial correlation for coded hyperspectral image restoration. In *CVPR*, pages 3727–3736, 2016. [2](#)
- [23] Wei Hu, Yangyu Huang, Li Wei, Fan Zhang, and Hengchao Li. Deep convolutional neural networks for hyperspectral image classification. *Journal of Sensors*, 2015:1–12, 2015. [1](#)
- [24] Jiaojiao Li, Chaoxiong Wu, Rui Song, Yunsong Li, and Fei Liu. Adaptive weighted attention network with camera spectral sensitivity prior for spectral reconstruction from rgb images. In *CVPRW*, pages 462–463, 2020. [2](#), [6](#)
- [25] Jiaojiao Li, Songcheng Du, Chaoxiong Wu, Yihong Leng, Rui Song, and Yunsong Li. Drcr net: Dense residual channel re-calibration network with non-local purification for spectral super resolution. In *CVPR*, pages 1259–1268, 2022. [2](#), [6](#)
- [26] Miaoyu Li, Ying Fu, Ji Liu, and Yulun Zhang. Pixel adaptive deep unfolding transformer for hyperspectral image reconstruction. In *ICCV*, pages 12959–12968, 2023. [1](#), [2](#)
- [27] Miaoyu Li, Ying Fu, and Yulun Zhang. Spatial-spectral transformer for hyperspectral image denoising. In *AAAI*, pages 1368–1376, 2023. [2](#), [3](#)
- [28] Yanyu Li, Geng Yuan, Yang Wen, Ju Hu, Georgios Evangelidis, Sergey Tulyakov, Yanzhi Wang, and Jian Ren. Efficientformer: Vision transformers at mobilenet speed. *NeurIPS*, 35:12934–12949, 2022. [3](#)
- [29] Yawei Li, Yuchen Fan, Xiaoyu Xiang, Denis Demandolx, Rakesh Ranjan, Radu Timofte, and Luc Van Gool. Efficient and explicit modelling of image hierarchies for image restoration. In *CVPR*, pages 18278–18289, 2023. [3](#)

- [30] Jie Liang, Jun Zhou, Xiao Bai, and Yuntao Qian. Salient object detection in hyperspectral imagery. In *ICIP*, pages 2393–2397. IEEE, 2013. 1
- [31] Jingyun Liang, Jie Zhang Cao, Guolei Sun, Kai Zhang, Luc Van Gool, and Radu Timofte. Swinir: Image restoration using swin transformer. In *ICCV*, pages 1833–1844, 2021. 3
- [32] Qian Liu, Zebin Wu, Yang Xu, and Zhihui Wei. A unified attention paradigm for hyperspectral image classification. *IEEE TGRS*, 61:1–16, 2023. 2, 3
- [33] Ze Liu, Yutong Lin, Yue Cao, Han Hu, Yixuan Wei, Zheng Zhang, Stephen Lin, and Baining Guo. Swin transformer: Hierarchical vision transformer using shifted windows. In *ICCV*, pages 10012–10022, 2021. 3
- [34] Patrick Llull, Xuejun Liao, Xin Yuan, Jianbo Yang, David Kittle, Lawrence Carin, Guillermo Sapiro, and David J Brady. Coded aperture compressive temporal imaging. *Optics express*, 21(9):10526–10545, 2013. 2
- [35] Zhihe Lu, Sen He, Xiatian Zhu, Li Zhang, Yi-Zhe Song, and Tao Xiang. Simpler is better: Few-shot semantic segmentation with classifier weight transformer. In *ICCV*, pages 8741–8750, 2021. 3
- [36] Farid Melgani and Lorenzo Bruzzone. Classification of hyperspectral remote sensing images with support vector machines. *IEEE TGRS*, 42(8):1778–1790, 2004. 1
- [37] Zhan Shi, Chang Chen, Zhiwei Xiong, Dong Liu, and Feng Wu. Hscnn+: Advanced cnn-based hyperspectral recovery from rgb images. In *CVPRW*, pages 939–947, 2018. 2, 6
- [38] Robin Strudel, Ricardo Garcia, Ivan Laptev, and Cordelia Schmid. Segmenter: Transformer for semantic segmentation. In *ICCV*, pages 7262–7272, 2021. 3
- [39] Ashish Vaswani, Noam Shazeer, Niki Parmar, Jakob Uszkoreit, Llion Jones, Aidan N Gomez, Łukasz Kaiser, and Illia Polosukhin. Attention is all you need. *NeurIPS*, 30, 2017. 2
- [40] Hongyuan Wang, Lizhi Wang, Chang Chen, Xue Hu, Fenglong Song, and Hua Huang. Learning spectral-wise correlation for spectral super-resolution: Where similarity meets particularity. In *ACM MM*, page 7676–7685, New York, NY, USA, 2023. Association for Computing Machinery. 2
- [41] Jiamian Wang, Kunpeng Li, Yulun Zhang, Xin Yuan, and Zhiqiang Tao. S²-transformer for mask-aware hyperspectral image reconstruction. *arXiv preprint arXiv:2209.12075*, 2022. 2, 3
- [42] Lizhi Wang, Chen Sun, Ying Fu, Min H Kim, and Hua Huang. Hyperspectral image reconstruction using a deep spatial-spectral prior. In *CVPR*, pages 8032–8041, 2019. 2
- [43] Lizhi Wang, Chen Sun, Maoqing Zhang, Ying Fu, and Hua Huang. Dnu: Deep non-local unrolling for computational spectral imaging. In *CVPR*, pages 1661–1671, 2020. 1, 2
- [44] Zhendong Wang, Xiaodong Cun, Jianmin Bao, Wengang Zhou, Jianzhuang Liu, and Houqiang Li. Uformer: A general u-shaped transformer for image restoration. In *CVPR*, pages 17683–17693, 2022. 3
- [45] Jie Xiao, Xueyang Fu, Aiping Liu, Feng Wu, and Zheng-Jun Zha. Image de-raining transformer. *IEEE TPAMI*, 2022. 3
- [46] Enze Xie, Wenhai Wang, Zhiding Yu, Anima Anandkumar, Jose M Alvarez, and Ping Luo. Segformer: Simple and efficient design for semantic segmentation with transformers. *NeurIPS*, 34:12077–12090, 2021. 3
- [47] Zhiwei Xiong, Zhan Shi, Huiqun Li, Lizhi Wang, Dong Liu, and Feng Wu. Hscnn: Cnn-based hyperspectral image recovery from spectrally undersampled projections. In *ICCVW*, pages 518–525, 2017. 1, 2
- [48] Jize Xue, Yong-Qiang Zhao, Yuanyang Bu, Wenzhi Liao, Jonathan Cheung-Wai Chan, and Wilfried Philips. Spatial-spectral structured sparse low-rank representation for hyperspectral image super-resolution. *IEEE TIP*, 30:3084–3097, 2021. 1, 2
- [49] Weihao Yu, Mi Luo, Pan Zhou, Chenyang Si, Yichen Zhou, Xinchao Wang, Jiashi Feng, and Shuicheng Yan. Metaformer is actually what you need for vision. In *CVPR*, pages 10819–10829, 2022. 3
- [50] Xin Yuan. Generalized alternating projection based total variation minimization for compressive sensing. In *ICIP*, pages 2539–2543. IEEE, 2016. 2
- [51] Xin Yuan, Yang Liu, Jinli Suo, and Qionghai Dai. Plug-and-play algorithms for large-scale snapshot compressive imaging. In *CVPR*, pages 1447–1457, 2020. 2
- [52] Xin Yuan, David J Brady, and Aggelos K Katsaggelos. Snapshot compressive imaging: Theory, algorithms, and applications. *IEEE Signal Processing Magazine*, 38(2):65–88, 2021. 1, 2
- [53] Syed Waqas Zamir, Aditya Arora, Salman Khan, Munawar Hayat, Fahad Shahbaz Khan, and Ming-Hsuan Yang. Restormer: Efficient transformer for high-resolution image restoration. In *CVPR*, pages 5728–5739, 2022. 3, 6
- [54] Jingang Zhang, Runmu Su, Qiang Fu, Wenqi Ren, Felix Heide, and Yunfeng Nie. A survey on computational spectral reconstruction methods from rgb to hyperspectral imaging. *Scientific reports*, 12(1):11905, 2022. 1
- [55] Shipeng Zhang, Lizhi Wang, Ying Fu, Xiaoming Zhong, and Hua Huang. Computational hyperspectral imaging based on dimension-discriminative low-rank tensor recovery. In *ICCV*, pages 10183–10192, 2019. 2
- [56] Shipeng Zhang, Lizhi Wang, Lei Zhang, and Hua Huang. Learning tensor low-rank prior for hyperspectral image reconstruction. In *CVPR*, pages 12006–12015, 2021. 2
- [57] Xianyi Zhang and Haitao Zhao. Hyperspectral-cube-based mobile face recognition: A comprehensive review. *Information Fusion*, 74:132–150, 2021. 1
- [58] Haiyu Zhao, Yuanbiao Gou, Boyun Li, Dezhong Peng, Jiancheng Lv, and Xi Peng. Comprehensive and delicate: An efficient transformer for image restoration. In *CVPR*, pages 14122–14132, 2023. 3
- [59] Yuzhi Zhao, Lai-Man Po, Qiong Yan, Wei Liu, and Tingyu Lin. Hierarchical regression network for spectral reconstruction from rgb images. In *CVPRW*, pages 422–423, 2020. 6
- [60] Wenbin Zou, Tian Ye, Weixin Zheng, Yunchen Zhang, Liang Chen, and Yi Wu. Self-calibrated efficient transformer for lightweight super-resolution. In *CVPR*, pages 930–939, 2022. 3